www.ietdl.org

Published in IET Control Theory and Applications
Received on 7th March 2010
Revised on 28th March 2012
doi: 10.1049/iet-cta.2010.0117

ISSN 1751-8644

A unified dual-stage actuator control scheme for track seeking and following in hard disk drives

J. Zheng[1] *M. Fu*[2]

[1] *Faculty of Engineering and Industrial Sciences, Swinburne University of Technology, Hawthorn, VIC 3122, Australia*
[2] *School of Control Science and Engineering, Zhejiang University, Hangzhou 310058, People's Republic of China*
E-mail: jzheng@swin.edu.au

Abstract: This paper presents a unified approach to track seeking and following control for a dual-stage actuator (DSA) hard disk drive (HDD) system. Based on a doubly coprime factorisation (DCF) method, the DSA controller and the closed-loop dynamics are expressed explicitly in terms of two design parameters. This greatly simplifies the optimisation of design parameters in meeting desired specifications. We then address how to use the design parameters to deal with specific problems in the DSA, that is, control allocation for disturbance rejection and trajectory planning for track seeking. Simulated results are also presented to verify the effectiveness of the proposed DSA controller. Compared with previous works, the proposed approach can fulfil track seeking and following tasks by a single controller without switching. Moreover, the unified controller can achieve desirable performances for both tasks that are equivalent to that by two separate conventional controllers.

1 Introduction

Hard disk drives (HDDs) are the most popular and cost-effective data storage devices nowadays. New technologies are being developed to meet the ever increasing demands for high-capacity and fast data rate HDDs [1]. From the perspective of control engineers, these demands can be translated into the technical specifications that the head position should be accurately maintained along the track centre (track-following mode) and swiftly moved from one track to another (track-seeking mode). Traditionally, the HDD head positioner is driven by a voice coil motor (VCM), which however, cannot provide the stringent performance any longer because of its mechanical resonance modes, various disturbances and noises in HDDs. Therefore the dual-stage actuator (DSA) HDDs are introduced to overcome these limitations [2, 3]. In DSA servo systems, the VCM actuator is used as the primary stage to provide long track seeking but with poor accuracy and slow response time, whereas the secondary stage such as a piezoelectric (PZT) microactuator [4] is used to provide higher precision and faster response but with a stroke limit. By combining the DSA system with properly designed controllers, the overall servo bandwidth of the head positioning mechanism can be significantly increased. Thereby, the DSA HDD system can achieve fast track seeking and allow ultra-high track density, which are far beyond the capability of conventional single-stage HDDs.

The control design for a DSA system is a much greater challenging task than for a conventional single-stage servo with VCM only. This is mainly because a DSA system is a dual-input single-output (DISO) system, which means that for a given desired trajectory, alternative inputs to the two actuators are not unique. Thus, a proper control strategy is required for control allocation in response to external inputs. Otherwise, the two actuators may fight each other and deteriorate the performance instead. A number of approaches have been reported for the DSA control problems. For example, control design for track following and settling can be found in [5–10]. In [11], a decoupled track-seeking controller using a three-step design approach is developed to enable high-speed one-track seeking and short-span track seeking for a dual-stage servo system. Short and long-span seeking controls are incorporated in a single-control scheme with fast settling time [12–14]. Further, the control design for the DSA including the interaction between both actuators is proposed in [15, 16] to attain desired time and frequency responses by minimising a new performance index, destructive interference, which was inrextroduced to express the degree of cooperation between both actuator systems with very different specifications and characteristics.

In most of the previous works, the control designs are focused on individual control problems for either track following or track seeking in HDDs. Accordingly, there needs a mode switching between the controllers for different control tasks. For this purpose, it is typical to employ the initial value compensation method [17] to achieve a smooth switching. This obviously results in extra implementation complexity. To avoid this situation, this paper introduces a unified design method for DSA track seeking and following control. The control design is based on the doubly coprime factorisation (DCF) approach [18], which provides the advantages that: (i) it parameterises all linear internally stabilised a two-degree-of-freedom (2-DOF) controller by two free design parameters; (ii) it

offers a unified design method to solve the seeking and disturbance rejection problems; (iii) the derived transfer functions of disturbance rejection response and seeking response are simply expressed and they are unique in terms of the design parameters, which makes the relationship between the design parameters and the desired specifications explicit.

Compared with the existing DSA control methods, the proposed 2-DOF controller explicitly addresses both track seeking and disturbance rejection problems in a unified design framework and it is easy to implement. In this paper, we focus on the development of the DSA controller for disturbance rejection and step tracking in the PZT range. For track seeking beyond the PZT range, the PZT has little use for reducing the seeking time because of its limited stroke. As such, it is typical to activate the VCM servo only to perform the long seeking task; see [13, 19] for example.

Throughout this paper, we use the following notation: for any signal $u(t)$, we denote its Laplace transform by $\hat{u}(s)$ or $\hat{u}$ for short; $\mathcal{RH}_\infty$ denotes the set of all stable, proper and rational transfer function matrices.

2 Plant and disturbance models

In this paper, we study the control design for a kind of DSA HDDs with a push–pull PZT micro-actuated suspension, a picture of which is shown in Fig. 1. It consists of a VCM actuator as the primary stage and a PZT actuator as the secondary stage. The PZT is located between the suspension and the E-block, which is moved by the VCM. The two actuators are, respectively, driven through a PZT amplifier and a VCM driver. The controlled variable is the head position, which is the only measurable signal for feedback control.

The mathematical modelling of DSAs has been well studied in [15, 20], where a simplified state-space model of the DSA was derived, that included a dominant PZT flexible mode dynamics and the interaction between both actuators. Here, we adopt the DSA model given in [15] as the plant model for the design and validation of our controller. To begin with, we reasonably assume that the PZT stroke limit (say, 1 μm) and inertia are very small relative to the VCM such that the dynamic interaction from the PZT to the VCM can be negligible. As such, the DSA plant model is given by

$$\begin{bmatrix}\hat{y}_\mathrm{v}\\ \hat{y}_\mathrm{p}\end{bmatrix}=\begin{bmatrix}G_\mathrm{v} & 0\\ G_\mathrm{pv} & G_\mathrm{p}\end{bmatrix}\begin{bmatrix}\hat{u}_\mathrm{v}\\ \hat{u}_\mathrm{p}\end{bmatrix} \tag{1}$$

$$y=y_\mathrm{v}+y_\mathrm{p} \tag{2}$$

where y_v, y_p, y, u_v and u_p denote the VCM displacement, the PZT displacement relative to VCM, the head displacement, the VCM control input and the PZT control input, respectively. G_v, G_p and G_pv represent the transfer functions of the VCM, PZT and the dynamic interaction from the VCM to the PZT, respectively. Furthermore, according to [15], the interaction model equals to

$$G_\mathrm{pv}=\varepsilon G_\mathrm{p}=-\left(1+\frac{l_\mathrm{p}}{r_\mathrm{p}}\right)\frac{K_\mathrm{v}J_\mathrm{p}}{J_\mathrm{v}K_\mathrm{p}}G_\mathrm{p} \tag{3}$$

where K_v and J_v are the torque constant and inertial of VCM; likewise, K_p and J_p are the counterpart of PZT; l_p and r_p are the length of PZT and the length from the PZT rotational point to the PZT mass centre; and ε denotes the constant coefficient $-(1+l_\mathrm{p}/r_\mathrm{p})(K_\mathrm{v}J_\mathrm{p}/J_\mathrm{v}K_\mathrm{p})$, respectively. Apparently, the position error contributed by the interaction G_pv becomes negligible in the case of $(K_\mathrm{v}J_\mathrm{p}/J_\mathrm{v}K_\mathrm{p}) \ll u_\mathrm{p}/u_\mathrm{v}$ [15].

To decouple the DSA model (1)–(2), define the control input transformation [20] as follows

$$u_1=u_\mathrm{v} \tag{4}$$

$$u_2=u_\mathrm{p}+\varepsilon u_\mathrm{v} \tag{5}$$

and rewrite $y_1=y_\mathrm{v}$, $y_2=y_\mathrm{p}$, $G_1=G_\mathrm{v}$ and $G_2=G_\mathrm{p}$. Then, we can transform the DSA model as

$$\begin{bmatrix}\hat{y}_1\\ \hat{y}_2\end{bmatrix}=\begin{bmatrix}G_1 & 0\\ 0 & G_2\end{bmatrix}\begin{bmatrix}\hat{u}_1\\ \hat{u}_2\end{bmatrix} \tag{6}$$

$$y=y_1+y_2 \tag{7}$$

We can see that the model in (6)–(7) is decoupled and apparently would facilitate the control design. Hence, combining (6)–(7) can lead to the overall DSA model $\boldsymbol{G}$ expressed by a decoupled DISO linear system

$$\hat{y}=\boldsymbol{G}\hat{u}=[G_1 \quad G_2]\begin{bmatrix}\hat{u}_1\\ \hat{u}_2\end{bmatrix} \tag{8}$$

The model parameters of G_1 and G_2 are given in the Appendix. Further, the frequency responses of G_1, G_2 and the interaction G_pv are shown in Fig. 2. From now on, we will take the DSA system in (8) as the plant model for control design.

The disturbance sources in HDDs that result in track-following errors contain both repeatable runout (RRO) and non-repeatable runout (NRRO). In this paper, we will design the controller to reject the disturbances that are reconstructed from a real HDD measurement. Fig. 3 shows the power spectra of the RROs and NRROs extracted from the disturbances. We can see that the RRO spectra include the harmonics with a fundamental frequency of 80 Hz that are associated with the spindle rotation frequency and the written-in RRO while servo writing. On the other hand, the NRROs contain narrow-band spectra around 644 Hz that are caused by the disk flutter and external shock and vibrations. In what follows, the controller will be designed to dedicate to rejecting these RROs and NRROs for reducing the overall position error signal (PES).

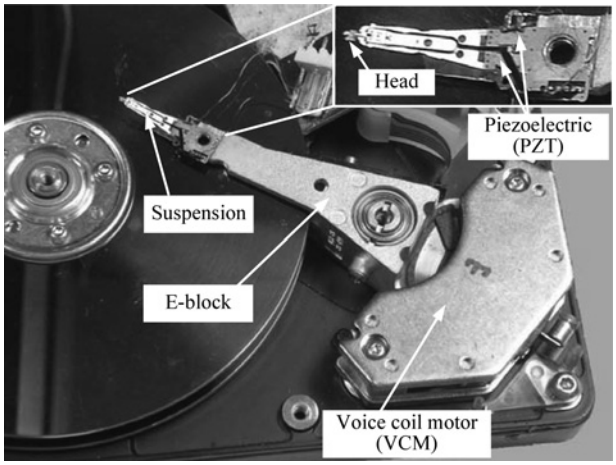

Fig. 1 *Picture of DSA HDDs with a PZT micro-actuated suspension*

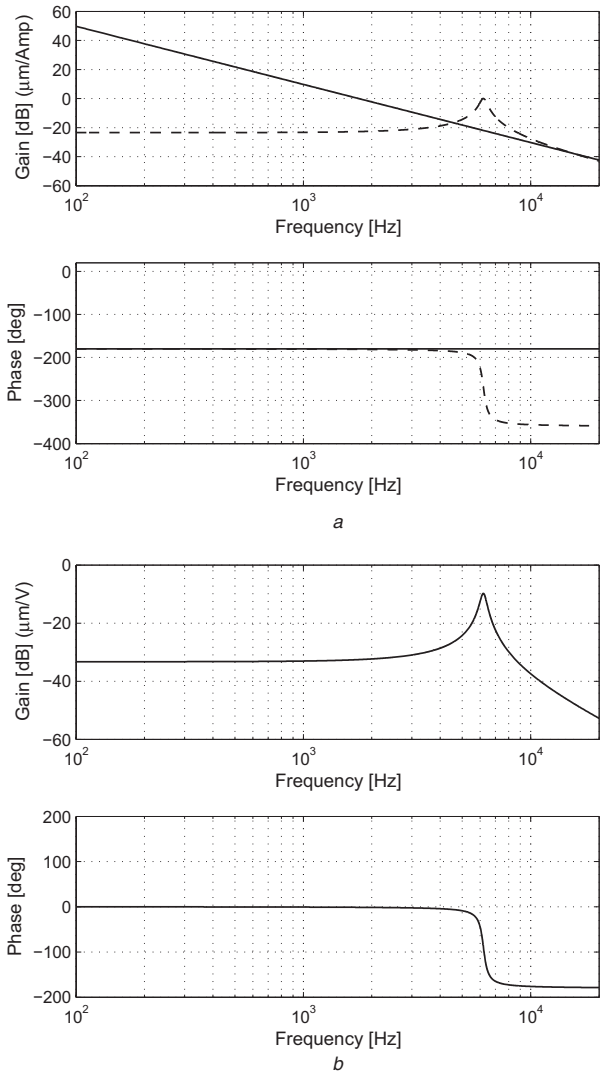

Fig. 2 *Frequency responses of the DSA model*

a Solid lines: VCM actuator G_1; dashed lines: interaction G_{pv}

b PZT actuator, G_2

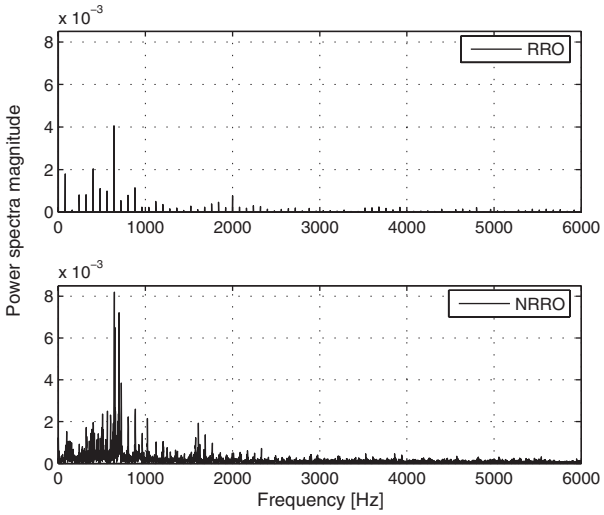

Fig. 3 *Power spectra of disturbances in a real HDD*

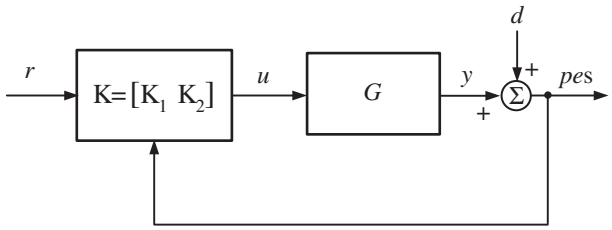

Fig. 4 *Generic 2-DOF control system for the DSA HDD*

3 Unified DSA control scheme

This section presents the fundamental design concept of a parameterised 2-DOF controller based on the DCF method, and then the design of the controller parameters is addressed to solve the DSA control problems of disturbance rejection and track seeking, respectively. The ultimate design results can straightforwardly yield a unified DSA controller for track-seeking and following modes in HDDs.

3.1 Fundamental design concept

Fig. 4 depicts a generic 2-DOF control structure for the DSA HDD system, where $\boldsymbol{G}$ denotes the DSA plant, $\boldsymbol{K}$ the 2-DOF controller to be designed, and the signals r, y, pes, $\boldsymbol{u}$ and d represent, respectively, the seeking reference, the head position, the PES, the control inputs, and the disturbance. In this setup, $\boldsymbol{K}$ is essentially a 2-DOF controller with $\boldsymbol{K_1}$ the feedforward controller and $\boldsymbol{K_2}$ the feedback controller. By using the coprime factorisation approach [18], we can parameterise the controller concisely. Let the right and left coprime factorisations of $\boldsymbol{G}$ be given by

$$\boldsymbol{G} = \boldsymbol{N}\boldsymbol{D}^{-1} = \tilde{D}^{-1}\tilde{\boldsymbol{N}} \tag{9}$$

where $\boldsymbol{N}$, $\boldsymbol{D}$, $\tilde{\boldsymbol{N}}$, $\tilde{D} \in \mathcal{RH}_\infty$ and satisfy the doubly Bezout identify

$$\begin{bmatrix} \tilde{\boldsymbol{X}} & -\tilde{\boldsymbol{Y}} \\ -\tilde{\boldsymbol{N}} & \tilde{D} \end{bmatrix} \begin{bmatrix} \boldsymbol{D} & \boldsymbol{Y} \\ \boldsymbol{N} & X \end{bmatrix} = I \tag{10}$$

for some X, $\boldsymbol{Y}$, $\tilde{\boldsymbol{X}}$, $\tilde{\boldsymbol{Y}} \in \mathcal{RH}_\infty$. A simple DCF representation of the DSA model is given in the Appendix. Hence, the class of all linear internally stabilising 2-DOF controllers $\boldsymbol{K} = [\boldsymbol{K_1} \quad \boldsymbol{K_2}]$ can be parameterised by

$$\hat{\boldsymbol{u}} = \boldsymbol{K_1}\hat{r} + \boldsymbol{K_2}\hat{pes} \tag{11}$$

$$\boldsymbol{K_1} = (\tilde{\boldsymbol{X}} - \boldsymbol{R}\tilde{\boldsymbol{N}})^{-1}\boldsymbol{Q} \tag{12}$$

$$\boldsymbol{K_2} = (\tilde{\boldsymbol{X}} - \boldsymbol{R}\tilde{\boldsymbol{N}})^{-1}(\tilde{\boldsymbol{Y}} - \boldsymbol{R}\tilde{D}) \tag{13}$$

where $\boldsymbol{Q}$ and $\boldsymbol{R}$ belonging to $\mathcal{RH}_\infty$, are the free parameters to be designed. By substituting the controllers $\boldsymbol{K_1}$ and $\boldsymbol{K_2}$ and the factorised plant model (9) into Fig. 4, we can easily obtain the following input–output relationship in frequency domain

$$\hat{pes} = T\hat{r} + S\hat{d} \tag{14}$$

with

$$T = \boldsymbol{N}\boldsymbol{Q}$$

$$S = (X - \boldsymbol{N}\boldsymbol{R})\tilde{D}$$

where T denotes the DSA closed-loop transfer function from the reference to the PES, and S the DSA sensitivity function

doi: 10.1049/iet-cta.2010.0117

from the disturbance to the PES. It is advantageous that both transfer functions are expressed by the design parameters $\boldsymbol{Q}$ and $\boldsymbol{R}$ explicitly.

Now, it is obvious that achieving the optimal performance of track seeking and following is equivalent to selecting a pair of $\boldsymbol{R}$ and $\boldsymbol{Q}$ such that $S \equiv 0$ and $T \equiv 1$, which, however, requires the conditions that the plant must be proper, right invertible, stable and minimum phase, and the resulting $\boldsymbol{R}$ and $\boldsymbol{Q}$ are proper. In most practical mechanisms including the HDDs, these strict conditions are rarely satisfied at the same time. Consequently, the designer has to deal with one or more of these constraints; and thereby it is more often that only $S \to 0$ and $T \to 1$ is achievable in the frequency range of interest [21]. In the following, based on the knowledge of the HDD dynamics and the disturbance characteristics, we shall propose a suboptimal design of $\boldsymbol{R}$ and $\boldsymbol{Q}$ that can overcome the constraints at hand while provide desirable fast track seeking and superior disturbance rejection in a wide frequency range.

3.2 Design of $\boldsymbol{R}$ for disturbance rejection

The design goal of $\boldsymbol{R}$ is to make the sensitivity function S have sufficiently low gains at the frequencies where the dominant disturbances situate. In addition, $\boldsymbol{R}$ should be capable of allocating the control efforts of the two actuators in response to disturbances at a different frequency range. Let $\boldsymbol{R} = [R_1 \quad R_2]^{\mathrm{T}}$ and $\boldsymbol{N} = [N_1 \quad N_2]$. We then introduce two new stable and proper transfer functions W and Φ, and a scalar β, and take

$$R_1 = \frac{X}{N_1}(1 - W)\Phi\beta \tag{15}$$

$$R_2 = \frac{X}{N_2}(1 - W)\Phi(1 - \beta) \tag{16}$$

where W depicts desirable gain attenuation at the target disturbance frequencies, β is a scalar for tuning the control allocation of the two actuators in response to the disturbances, Φ is a low-pass filter with unity gain within the frequency range of interest, and its order is chosen to make both R_1 and R_2 proper so that the resulting controller is implementable. Now, with $\boldsymbol{R}$ expressed by (15)–(16), we have

$$\begin{aligned} S &= X\tilde{D}(1 - \Phi + \Phi W) \\ &\approx X\tilde{D}W. \quad (\text{as } \Phi \approx 1) \end{aligned} \tag{17}$$

Denote the term $X\tilde{D}$ as the nominal DSA sensitivity function

$$S^N = X\tilde{D} \tag{18}$$

which actually results from a corresponding nominal controller by setting $\boldsymbol{R} = \boldsymbol{0}$. Now, from (17)–(18), we can see that S is simply the multiplication of S^N and W. In general, S^N is only capable of rejecting low-frequency disturbances because the nominal servo bandwidth has to be limited to provide sufficient stability margin. To further reject the narrow-band RROs and NRROs beyond the servo bandwidth, the design parameter W can thus be selected to have low gains at these specified frequencies. To do this, W can be given by

$$W = \prod_{i=1}^{n} \frac{s^2 + 2\zeta_{1i}\omega_i s + \omega_i^2}{s^2 + 2\zeta_{2i}\omega_i s + \omega_i^2}, \quad \zeta_{1i} < \zeta_{2i} \tag{19}$$

where n is the number of target disturbances for rejection, $\zeta_{1i}, \zeta_{2i} \in (0, 1)$ are the damping ratios, and ω_i is the centre frequency of RROs and NRROs. Apparently, the gains of W can be arbitrarily low at the disturbance frequencies by selecting appropriate pair (ζ_{1i}, ζ_{2i}).

It is also interesting to see from (17) that S is unrelated to β, which means that β can be chosen without affecting S. This is because the DSA is essentially an actuator-redundant system. However, as the VCM and PZT have quite different dynamics, a suitable β should be carefully selected to determine the control allocation of the two actuators in response to the disturbances. Typically, the VCM works mainly for the low-frequency movement, whereas the PZT responses more for high-frequency disturbances. A useful method to analyse the control allocation of the two actuators is investigating the ratio of the open-loop systems of the two actuators in frequency domain [5, 21]. Specifically, let the controller $\boldsymbol{K_2} = [K_{21} \quad K_{22}]^{\mathrm{T}}$, $\boldsymbol{Y} = [Y_1 \quad Y_2]^{\mathrm{T}}$, and define the open-loop systems of the VCM and PZT as $OL_1 = G_1K_{21}$ and $OL_2 = G_2K_{22}$, respectively. Then we can obtain the ratio of OL_1 and OL_2 as

$$\begin{aligned} \Gamma = \frac{OL_1}{OL_2} &= \frac{X(1 - W)\Phi\beta - Y_1G_1}{X(1 - W)\Phi(1 - \beta) - Y_2G_2} \\ &\simeq \frac{X(1 - W)\beta - Y_1G_1}{X(1 - W)(1 - \beta) - Y_2G_2} \end{aligned} \tag{20}$$

We can see that Γ is a function of β provided that W is determined. In order to make the two actuators have maximum cooperation, Γ is chosen to give a roll-off characteristics and its phases are less than 120° when its magnitudes are nearly one (0 dB). This means that when the outputs of VCM and PZT have nearly the same magnitude, the relative phases of VCM loop and PZT loop should be less than 120° such that the total DSA output is greater than one, and thus the two loops will not destructively interfere [5]. From (15)–(16), it can be intuitively seen that a smaller β indicates a larger relative contribution from the PZT than the VCM (see Fig. 8 later for illustration), but it also tends to saturate the PZT.

Finally, the Φ filter is taken with the following form [22]

$$\Phi = \frac{6\tau^2 s^2 + 4\tau s + 1}{\tau^4 s^4 + 4\tau^3 s^3 + +6\tau^2 s^2 + 4\tau s + 1} \tag{21}$$

where τ is the time constant that determines the filter bandwidth. Here, the numerator and denominator order of Φ are selected such that Φ has a best fit to unity in both gain and phase characteristics within the bandwidth and additionally R_1 and R_2 are made to be proper for practical implementation. Ideally, the frequency bandwidth of Φ should be extended as high as possible (by choosing a smaller τ) to achieve wide-band disturbance rejection. However, in practice, this desired performance has to be compromised with sensor noise suppression. As we can see in Fig. 4, the measured *pes* generally contains sensor noise, then the control input would be affected by the noise amplification through the feedback controller $\boldsymbol{K_2}$ involving a high bandwidth Φ filter. In view of this trade-off, it suffices to choose the filter bandwidth as 3–4 times of the DSA closed-loop system bandwidth.

3.3 Design of $\boldsymbol{Q}$ for track seeking

Let $\boldsymbol{Q} = [Q_1 \quad Q_2]^{\mathrm{T}}$. Owing to the fact that G_1 and G_2 are minimum phase, we thus aim at the design of Q_1 and Q_2 such that $T = N_1Q_1 + N_2Q_2 \to 1$ has a high-frequency bandwidth. Furthermore, it is required that the displacement of PZT settles down to zero at steady state. This means that $y_1(\infty) = r$ and $y_2(\infty) = 0$ should be satisfied for a step response with amplitude r assuming the disturbance with $d(\infty) = 0$. Hence, we first analyse the individual position outputs of the two actuators. Partition $\boldsymbol{D}$ as

$$\boldsymbol{D} = \begin{bmatrix} D_1 & 0 \\ 0 & D_2 \end{bmatrix} \tag{22}$$

and suppose $d = 0$, it is thus easy to obtain

$$\begin{aligned} \begin{bmatrix} \hat{y}_1 \\ \hat{y}_2 \end{bmatrix} &= \begin{bmatrix} G_1 & 0 \\ 0 & G_2 \end{bmatrix} \begin{bmatrix} \hat{u}_1 \\ \hat{u}_2 \end{bmatrix} \\ &= \begin{bmatrix} N_1D_1^{-1} & 0 \\ 0 & N_2D_2^{-1} \end{bmatrix} \boldsymbol{DQ}\hat{r} \\ &= \begin{bmatrix} N_1Q_1 \\ N_2Q_2 \end{bmatrix} \hat{r} \end{aligned} \tag{23}$$

We can see that the step responses of the two actuators are completely decoupled in terms of Q_1 and Q_2. As the transfer functions N_1 and N_2 are designed (by selecting proper $\boldsymbol{F}$ and $\boldsymbol{L}$ as discussed in the Appendix) to individually reflect the VCM and PZT closed-loop dynamics, we can then interpret Q_1 and Q_2 as the trajectory planning functions for the two actuators. We choose Q_1 and Q_2 as

$$Q_1 = N_1(0)^{-1} \tag{24}$$

$$Q_2 = \gamma N_2(0)^{-1}(1 - N_1N_1(0)^{-1}) \tag{25}$$

where $\gamma \in [0 \ \ 1]$ is a tuning scalar. It is obvious that $N_1(0)Q_1(0) = 1$ and $N_2(0)Q_2(0) = 0$, which imply that

$$y(\infty) = y_1(\infty) + y_2(\infty) = r + 0 = r \tag{26}$$

Moreover, define the VCM and PZT closed-loop systems by

$$T_1 = N_1N_1(0)^{-1} \tag{27}$$

$$T_2 = N_2N_2(0)^{-1} \tag{28}$$

We then obtain the DSA closed-loop transfer function as

$$T = T_1 + \gamma T_2(1 - T_1) \tag{29}$$

It is clear that when γ varies from 0 to 1, the cut-off frequency of T switches from that of T_1 to that of T_2 (e.g. see Fig. 9 for illustration). On the other hand, we can see from (25) that the PZT will follow the scaled tracking error of the VCM loop, that is, $\gamma(1 - N_1N_1(0)^{-1})r$, where γ actually determines the contribution of the PZT to the overall position output. Since the PZT has a faster response than the VCM loop, it is preferable to have a maximal position output of the PZT. Thus, we should maximise $\gamma \in [0 \ \ 1]$ subject to

$$\|T\|_\infty \le 0\,\mathrm{dB} \tag{30}$$

$$\|y_2\|_\infty \le 1.0\,\mu\mathrm{m} \tag{31}$$

where the constraint (30) is introduced for no overshoot in response to the track-seeking command in the PZT's range; and (31) is to avoid the saturation of the PZT (note that we assume the PZT's stroke limit is 1.0 μm).

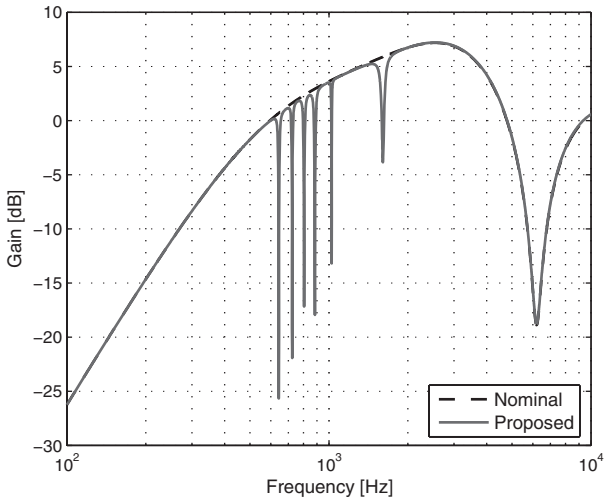

Fig. 5 *Frequency response of DSA sensitivity function*

4 Application and performance evaluation

In this section, we present a design example using the proposed control method. The performance of the controller is evaluated by simulations.

4.1 Design results

We use the DSA plant parameters as discussed in Section 2 and assume a track density of 25.4 kTPI (i.e. one-track pitch is 1 μm) for the design and simulation. Then, the 2-DOF controller for the DSA HDD servo system should satisfy the following specifications:

1. Track-following servo system achieving PES 3σ value less than 10% of a track pitch, that is, $\le 0.1\,\mu$m.
2. Track-seeking response with settling time less than 0.3 ms and overshoot less than 10% of a track. Moreover, the displacement of PZT should settle down to zero at steady state for further response to a sequential seeking command.
3. For robust stability, the DSA servo system should have gain margin larger than 5 dB and phase margin more than 40°.

For simplicity, we will present a step-by-step design procedure.

Step 1: DCF of $\boldsymbol{G}$
According to the factorisation approach in the Appendix, we first select $F_1 = [1.1746 \times 10^5 \ \ 56.1]$ and $L_1 = [5.65 \times 10^4 \ \ 9.8 \times 10^8]^{\mathrm{T}}$ to make the VCM loop and its estimator have a bandwidth of 600 and 3000 Hz, respectively, and select $F_2 = [-3.5362 \times 10^7 \ \ 955.7]$ and $L_2 = [8.8 \times 10^4 \ \ 7.88 \times 10^8]^{\mathrm{T}}$ for the counterparts of the PZT with 5 and 8 kHz bandwidths, respectively. Then, the DCF of $\boldsymbol{G}$ can be easily computed by (33)–(40). We can evaluate the nominal DSA servo system since it is only related to $\boldsymbol{F}$ and $\boldsymbol{L}$. Fig. 5 shows the nominal DSA sensitivity function indicating a 600 Hz crossover frequency. The dashed lines in Fig. 6 show the frequency response of the nominal DSA open-loop system, which indicates that a gain margin of 5 dB and a phase margin of 42° are obtained. By simulating the nominal DSA servo system in the presence of disturbances, we collect the PES samples and the corresponding power spectra is shown in Fig. 10*a*, which clearly indicates that the disturbances around the nominal servo bandwidth 600 Hz

doi: 10.1049/iet-cta.2010.0117

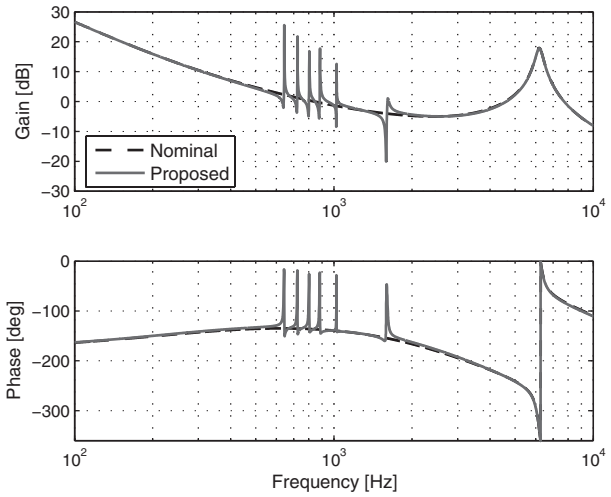

Fig. 6 *Frequency response of DSA open-loop system*

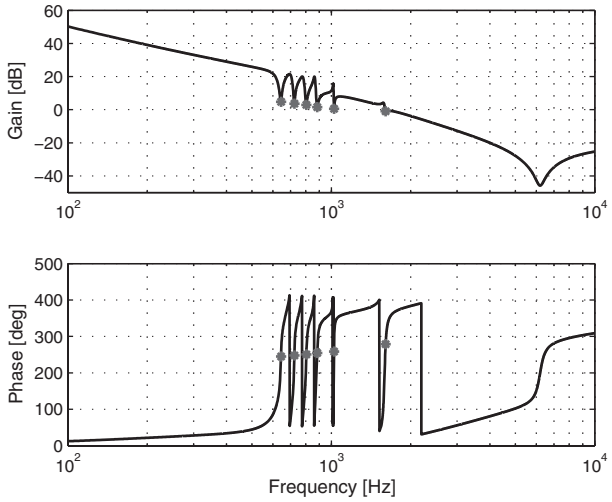

Fig. 7 *Bode plot of Γ function (The '⋆' indicates the frequency responses at the target disturbance frequencies)*

Table 1 Parameters of $W(s)$

i	ω_i	ζ_{1i}	ζ_{2i}
1	$2\pi \cdot 644$	5×10^{-4}	8×10^{-3}
2	$2\pi \cdot 724$	5×10^{-4}	6×10^{-3}
3	$2\pi \cdot 804$	1×10^{-3}	8×10^{-3}
4	$2\pi \cdot 884$	1×10^{-3}	9×10^{-3}
5	$2\pi \cdot 1024$	5×10^{-4}	3×10^{-3}
6	$2\pi \cdot 1608$	8×10^{-3}	0.022

are not greatly compensated. Therefore, the design of $\boldsymbol{R}$ in the next step would be dedicated to the suppression of these disturbances.

Step 2: Design of $\boldsymbol{R}$

According to Fig. 10*a*, we aim at suppressing the dominant disturbances with peak frequencies of 644, 724, 804, 884, 1024 and 1680 Hz. First, we determine W in (19) by setting $n = 6$ and ω_i corresponding to each peak frequency. The smaller value of ζ_{1i} and a bigger relative ratio to ζ_{2i} can lead to a higher reduction ratio at the disturbance frequency. In our case, the values of these parameters are listed in Table 1. Second, we set $\beta = 0.3$ and $\tau = 1/2\pi 8000$ for the Φ filter. Finally, we can easily calculate $\boldsymbol{R}$ from (15)–(16).

The proposed DSA sensitivity function S is shown in Fig. 5 in comparison with the nominal one S^N. It is clear that the gains at the disturbance frequencies are greatly decreased without amplifying the gains at the neighbouring frequencies. The frequency response of the DSA open-loop system is shown in Fig. 6, which indicates that the proposed DSA controller provides high gains around the target disturbance frequencies. It should be noted that although these high gains lead to multiple 0-dB crossover frequencies, their corresponding phases are all above $-180°$ implying that the closed-loop system is still stable. This again verifies the benefit of the factorisation approach for sensitivity loop shaping with guaranteed stability. To verify the control allocation of the DSA, Fig. 7 shows the Bode plot of Γ function (20). We can see that the designed Γ has a roll-off characteristics, and especially at the target disturbance frequencies the magnitudes of Γ are nearly one and the corresponding phases are around 250°. In other words, the relative phases of the VCM and PZT loop are kept about 110°, which implies a friendly cooperation of the two actuators. In addition, Fig. 8 shows the frequency responses of Γ with respect to various β values, which indicates that the gain significantly decreases with a smaller β. This in turn leads to a larger disturbance rejection contribution from the PZT, but note that it also tends to saturate the PZT.

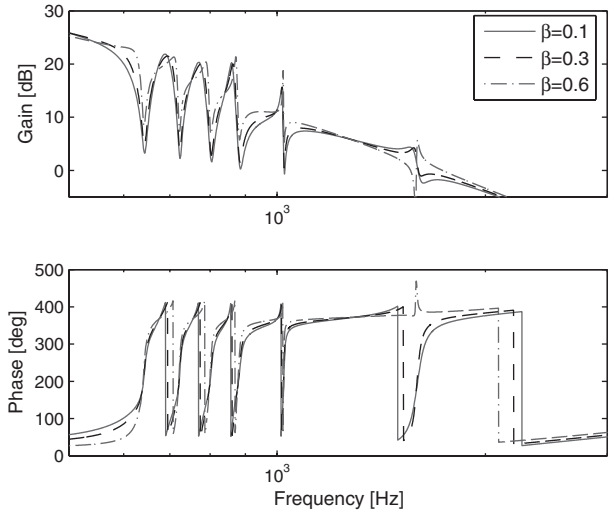

Fig. 8 *Comparison of Γ function illustrating DSA control allocation with respect to β*

Step 3: Design of $\boldsymbol{Q}$

For track-seeking control, we set $\gamma = 0.72$, and then $\boldsymbol{Q}$ can be obtained from (24)–(25). Fig. 9 shows the frequency responses of the closed-loop system of the DSA (T), the VCM (T_1), and the PZT (T_2), respectively. We can see that the DSA frequency bandwidth is located between that of the VCM loop and that of the PZT loop, which indicates that the DSA servo system should be faster than the VCM loop but slower than the PZT loop as expected. In addition, the maximal peak of T, that is, $\|T\|_\infty$, satisfies the design constraint (30) for no overshoot. Comparatively, a smaller γ, for example, 0.5, will result in a lower bandwidth; while a too large γ, for example, 0.9, will result in a larger $\|T\|_\infty$ indicating an excess overshoot.

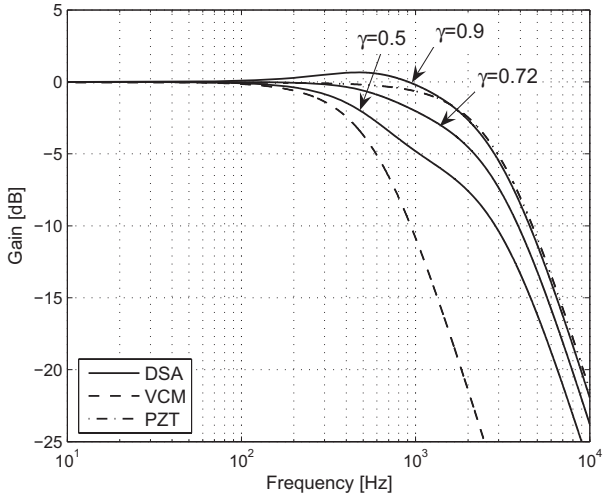

Fig. 9 *Frequency response of DSA closed-loop transfer function*

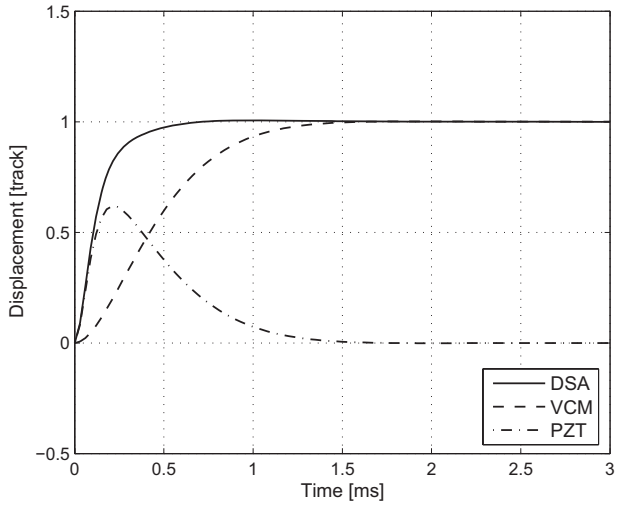

Fig. 11 *Time response to one track seeking*

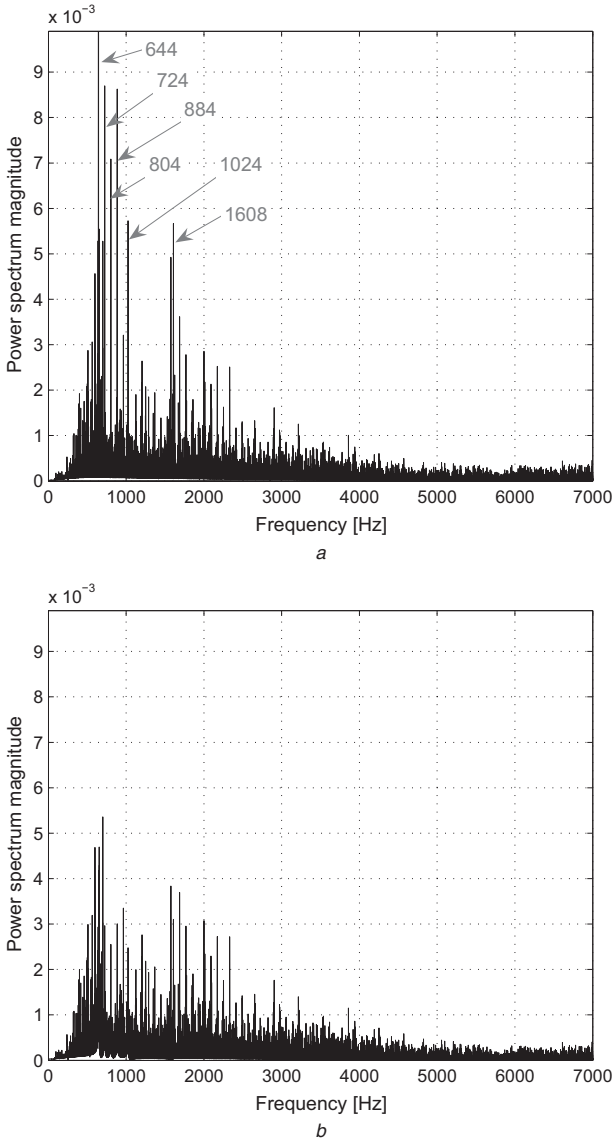

Fig. 10 *Power spectra of PES samples*

a Nominal DSA servo system with $\boldsymbol{R} = \mathbf{0}$ (PES $3\sigma = 0.1\,\mu$m). The arrows indicate the target NRROs to be rejected.

b Proposed DSA servo system (PES $3\sigma = 0.082\,\mu$m). The proposed DSA servo system achieves a 18% reduction ratio of PES-3σ value compared with the nominal DSA servo system

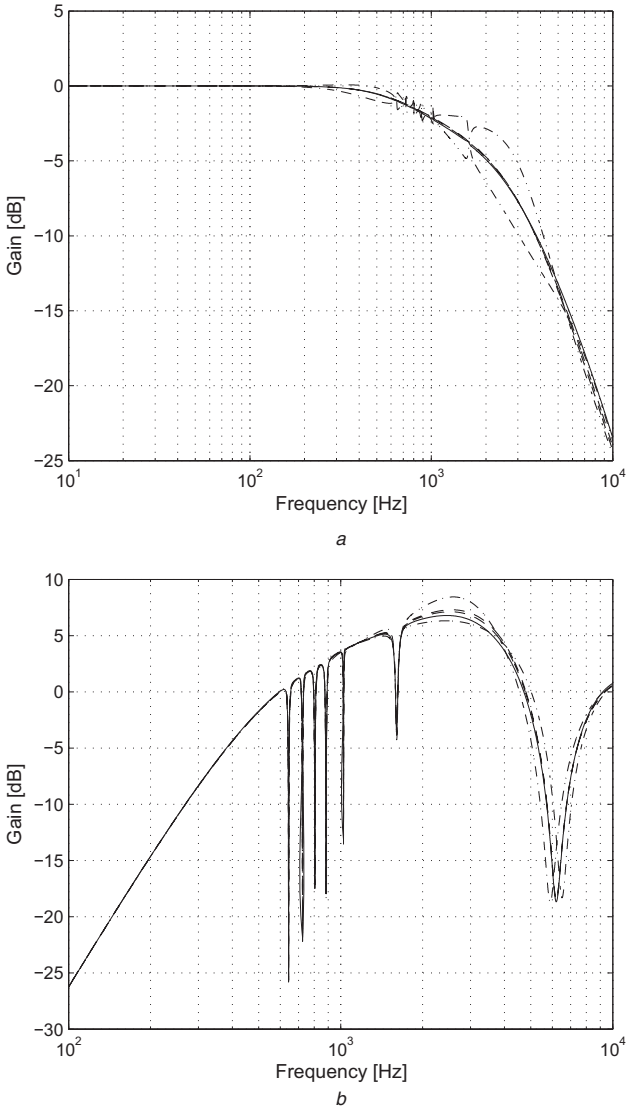

Fig. 12 *Frequency responses plots under the DSA plant model parameter uncertainties*

a Closed-loop transfer function

b Sensitivity function. (Solid lines: with unperturbed plant; dashed lines: with interaction model parameter ε variation of $\pm 20\%$; dash-dot lines: with PZT's resonant frequency variation of $\pm 5\%$.)

doi: 10.1049/iet-cta.2010.0117

4.2 Performance validation

The DSA control system is simulated using MATLAB/Simulink at a sampling frequency of 25 kHz. We first evaluate the track-following servo system by setting $r = 0$ and injecting the disturbances d characterised by Fig. 3. In this mode, only the feedback controller $\boldsymbol{K}_2$ takes action. The power spectra of the resultant PES is shown in Fig. 10. It is obvious that with the proposed DSA controller the target disturbances as specified in W (19) are remarkably rejected compared with those with nominal DSA controller (with $\boldsymbol{R} = \boldsymbol{0}$). The PES 3σ value is reduced from 0.1 to 0.082 μm, which is a 18% reduction ratio. Next, the one-track-seeking performance is evaluated by setting $r = 1$ μm and $d = 0$. In this mode, the feedforward controller $\boldsymbol{K}_1$ works to generate appropriate seeking trajectories for VCM and PZT, respectively. Fig. 11 shows the time response to one track seeking, which indicates that the settling time under the proposed DSA controller is only 0.3 ms considerably smaller than that of the VCM. Moreover, the selected γ ensures the PZT displacement is within its limit as required by (31). It should be noted that in real implementation, when the head position approaches the target track, the proposed unified controller does not require extra switching manipulation for transferring to the track-following mode.

We also note that the dynamic interaction is actually decoupled using a feedforward control input as shown in (5). As such, we further simulate the performance robustness against the interaction model parameter ε variation and the PZT's resonant frequency variation. Fig. 12 shows the frequency responses of the DSA closed-loop system and the sensitivity function, which indicate that the characteristic of the plots actually does not vary much when the plant is perturbed by the uncertainties. Moreover, Fig. 13 compares the performance robustness test results of the track seeking and following. It is clear that the performance is maintained within about 10% of the unperturbed servo system in all cases.

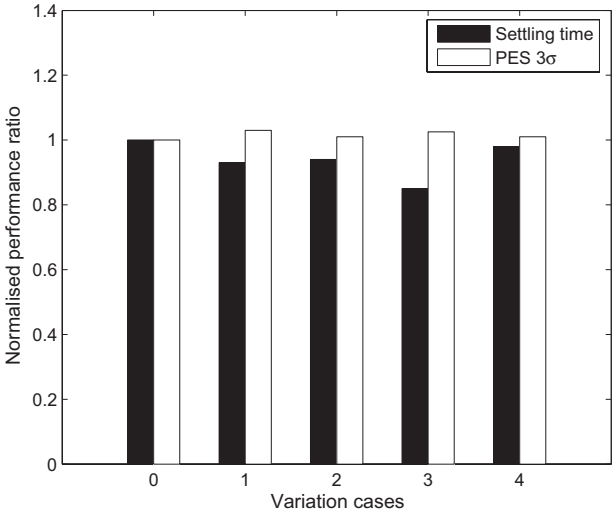

Fig. 13 *Performance robustness of the proposed controller against the DSA plant model parameter uncertainties (Case 0: with unperturbed plant; cases 1–2: with interaction model parameter ε variation of ±20%; cases 3–4: with PZT's resonant frequency variation of ±5%.)*

4.3 Comparative study

We also carry out a comparative study between the proposed unified controller and a conventional decoupled master–slave (DMS) controller [2]. In the DMS control scheme, the total DSA sensitivity function is the product of the VCM and PZT sensitivity functions. Hence, the controller design is decoupled into two independent loop designs for the VCM and PZT, respectively. Since the DMS controller is easy to design and offers basic performance, it is widely used as a baseline controller to investigate advanced DSA controllers (e.g. see [8, 9, 11, 23]). In our study, we design the DMS controller using a lead-lag controller for the VCM and a high DC-gain low-pass filter for the PZT. For the sake of fair comparison, the DMS controller is tuned to have similar servo bandwidth and stability margin as those of the proposed unified controller. Fig. 14 shows the comparison of the PES power spectra between two controllers. We can see that the achievable PES 3σ of conventional controller is a bit larger than that of the

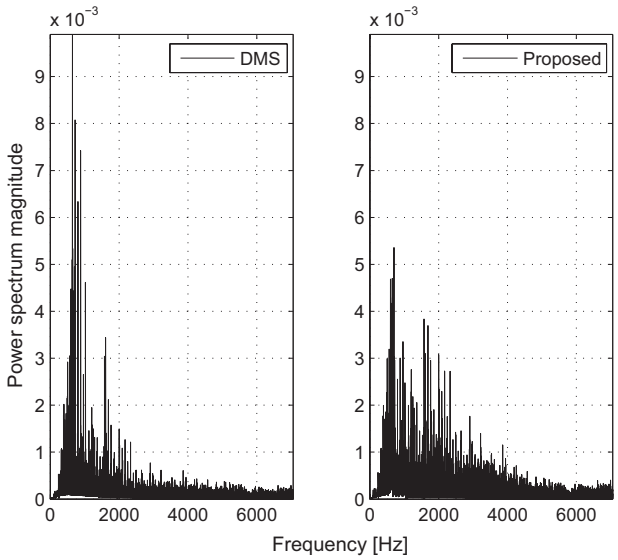

Fig. 14 *Comparison of PES power spectra (DMS: PES $3\sigma = 0.083$ μm; Proposed: PES $3\sigma = 0.082$ μm)*

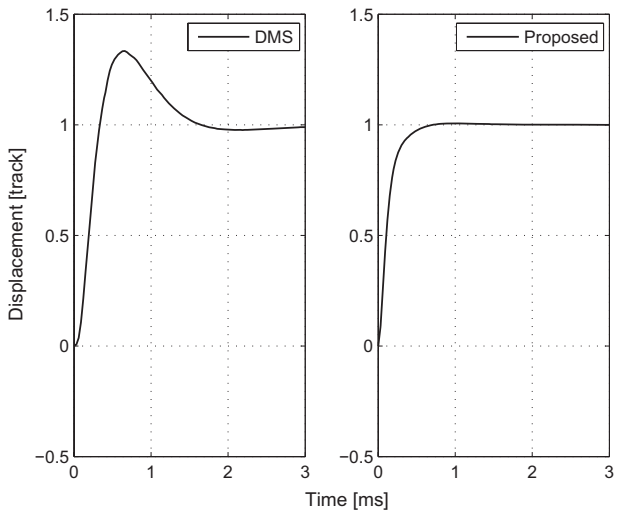

Fig. 15 *Comparison of one track seeking*
The DMS-based servo exhibits excess overshoot resulting in longer settling time

proposed controller because it lacks sufficient control efforts to reject the NRROs avout 800 Hz. The track-seeking comparison is also shown in Fig. 15, which indicates that the conventional controller results in a remarkably long settling time because of the excess overshoot. This is mainly because the conventional DMS controller is merely a single-degree-of-freedom controller, while the proposed unified controller combines a feedforward path to improve the seeking performance.

5 Conclusion

In this paper, we have developed a unified approach to track seeking and following control of a DSA HDD system. The design method can explicitly reflect the design criteria of fast seeking and disturbance rejection in terms of two design parameters. We further discuss the selection of the design parameters for proper DSA control allocation. Finally, simulation results are presented to verify the efficacy of the proposed controller. It can be concluded that the proposed unified controller can achieve desirable performances for both track seeking and following that are equivalent to that by two separate conventional controllers. The developed DSA HDD controller is comparatively simpler for implementation.

6 References

1 Wood, R., Takano, H.: 'Prospects for magnetic recording over the next 10 years'. Proc. IEEE Int. Magnetics Conf., 2006, p. 98
2 Mori, K., Munemoto, T., Otsuki, H., Yamaguchi, Y., Akagi, K.: 'A dual-stage magnetic disk drive actuator using a piezoelectric device for a high track density', *IEEE Trans. Magn.*, 1991, **27**, (6), pp. 298–5300
3 Imamura, T., Katayama, M., Ikegawa, Y., Ohwe, T., Koishi, R., Koshikawa, T.: 'MEMS-based integrated head/actuator/slider for hard disk drives', *IEEE/ASME Trans. Mechatron.*, 1998, **3**, (3), pp. 166–174
4 Evans, R., Griesbach, J., Messner, W.: 'Piezoelectric microactuator for dual stage control', *IEEE Trans. Magn.*, 1999, **35**, (2), pp. 977–982
5 Schroeck, S., Messner, W., McNab, R.: 'On compensator design for linear time-invariant dual-input single-output systems', *IEEE/ASME Trans. Mechatron.*, 2001, **6**, (1), pp. 50–57
6 Huang, X., Horowitz, R.: 'Robust controller design of a dual-stage disk drive servo system with an instrumented suspension', *IEEE Trans. Magn.*, 2005, **41**, (8), pp. 2406–2413
7 Du, C., Guo, G., Wu, D.: 'Low-hump sensitivity function design for dual-stage HDD systems with different microactuators', *IEE Proc. Control Theory Appl.*, 2005, **152**, (6), pp. 655–661
8 Guo, G., Wu, D., Chong, T.: 'Modified dual-stage controller for dealing with secondary-stage actuator saturation', *IEEE Trans. Magn.*, 2003, **39**, (6), pp. 3587–3592
9 Numasato, H., Tomizuka, M.: 'Settling control and performance of a dual-actuator system for hard disk drives', *IEEE/ASME Trans. Mechatron.*, 2003, **8**, (4), pp. 431–438
10 Thum, C., Du, C., Lewis, F., Chen, B., Ong, E.: 'H_∞ disturbance observer design for high precision track following in hard disk drives', *IET Control Theory Appl.*, 2009, **3**, (12), pp. 1591–1598
11 Kobayashi, M., Horowitz, R.: 'Track seek control for hard disk dual-stage servo systems', *IEEE Trans. Magn.*, 2001, **37**, (2), pp. 949–954
12 Hredzak, B., Herrmann, G., Guo, G.: 'A proximate-time-optimal control design and its application to a hard disk drive dual-stage actuator system', *IEEE Trans. Magn.*, 2006, **42**, (6), pp. 1708–1715
13 Zheng, J., Fu, M., Wang, Y., Du, C.: 'Nonlinear tracking control for a hard disk drive dual-stage actuator system', *IEEE/ASME Trans. Mechatron.*, 2008, **13**, (5), pp. 510–518
14 Li, H., Du, C., Wang, Y.: 'Optimal reset control for a dual-stage actuator system in HDDs', *IEEE/ASME Trans. Mechatron.*, 2011, **16**, (3), pp. 480–488
15 Lee, S., Kim, Y.: 'Minimum destructive interference design of dual-stage control systems for hard disk drives', *IEEE Trans. Contr. Syst. Technol.*, 2004, **12**, (4), pp. 517–531
16 Lee, S., Chung, C.: 'Optimal design and testing of a digital dual-stage actuator servo system', *IET Control Theory Appl.*, 2010, **4**, (10), pp. 2029–2040
17 Yamaguchi, T., Numasato, H., Hirai, H.: 'A mode-switching control for motion control and its application to disk drives: design of optimal mode-switching conditions', *IEEE/ASME Trans. Mechatron.*, 1998, **3**, (3), pp. 202–209
18 Vidyasagar, M.: 'Control system synthesis: a factorization approach', (MIT Press, Cambridge, MA, 1995)
19 Franklin, G.F., Powell, J.D., Emami-Naeini, A.: 'Feedback control of dynamic systems', (Addison-Wesley, Reading, MA, 1994, 3rd edn.)
20 Kim, Y., Lee, S.: 'An approach to dual-stage servo design in computer disk drives', *IEEE Trans. Control Syst. Technol.*, 2004, **12**, (1), pp. 12–20
21 Zheng, J., Su, W., Fu, M.: 'Tow-degree-of-freedom of control of a dual-stage actuator positioning system for short-span tracking'. Proc. American Control Conf., 2009, pp. 3681–3686
22 Choi, Y., Yang, K., Chung, W., Kim, H., Suh, I.: 'On the robustness and performance of disturbance observers for second-order systems', *IEEE Trans. Autom. Control*, 2003, **48**, (2), pp. 315–320
23 Guo, L., Martin, D., Brunnett, D.: 'Dual-stage actuator servo control for high density disk drives'. Proc. IEEE/ASME Int. Conf. Advanced Intelligent Mechatronics, 1999, pp. 132–137
24 Nett, C., Jacobson, C., Balas, M.: 'A connection between state-space and doubly coprime fractional representations', *IEEE Trans. Autom. Control*, 1984, **AC-29**, (9), pp. 831–832

7 Appendix: A factorisation representation of the DSA model

First, let the DSA model $\boldsymbol{G(s)}$ in (8) be represented in a state-space realisation as follows

$$\boldsymbol{G}(s) = \boldsymbol{C}(s\boldsymbol{I} - \boldsymbol{A})^{-1}\boldsymbol{B} \tag{32}$$

where

$$\boldsymbol{A} = \left[\begin{array}{c|c} \boldsymbol{A_1} & 0 \\ \hline 0 & \boldsymbol{A_2} \end{array}\right] = \left[\begin{array}{cc|cc} 0 & 1 & 0 & 0 \\ 0 & 0 & 0 & 0 \\ \hline 0 & 0 & 0 & 1 \\ 0 & 0 & -1.52\times 10^9 & -2597 \end{array}\right]$$

$$\boldsymbol{B} = \left[\begin{array}{c|c} \boldsymbol{B_1} & 0 \\ \hline 0 & \boldsymbol{B_2} \end{array}\right] = \left[\begin{array}{c|c} 0 & 0 \\ 121 & 0 \\ \hline 0 & 1 \\ 0 & 32.88 \end{array}\right]$$

$$\boldsymbol{C} = \left[\begin{array}{c|c} \boldsymbol{C_1} & \boldsymbol{C_2} \end{array}\right] = \left[\begin{array}{cc|cc} 1 & 0 & 1 & 0 \end{array}\right]$$

and $(\boldsymbol{A_1}, \boldsymbol{B_1}, \boldsymbol{C_1})$ and $(\boldsymbol{A_2}, \boldsymbol{B_2}, \boldsymbol{C_2})$ are the state-space representations of the VCM model G_1 and PZT model G_2, respectively. Also, we have $\varepsilon = -3.1$ for the interaction model (3). Since the pairs $(\boldsymbol{A}, \boldsymbol{B})$ and $(\boldsymbol{A}, \boldsymbol{C})$ are stabilisable and detectable, respectively. we can select $\boldsymbol{F}$ and $\boldsymbol{L}$ such that $(\boldsymbol{A} - \boldsymbol{BF})$ and $(\boldsymbol{A} - \boldsymbol{LC})$ are both Hurwitz. Thus, a DCF of $\boldsymbol{G(s)}$ [24] is given by

$$\boldsymbol{N}(s) = \boldsymbol{C}(s\boldsymbol{I} - \boldsymbol{A} + \boldsymbol{BF})^{-1}\boldsymbol{B} \tag{33}$$

$$\boldsymbol{D}(s) = \boldsymbol{I} - \boldsymbol{F}(s\boldsymbol{I} - \boldsymbol{A} + \boldsymbol{BF})^{-1}\boldsymbol{B} \tag{34}$$

$$\tilde{\boldsymbol{N}}(s) = \boldsymbol{C}(s\boldsymbol{I} - \boldsymbol{A} + \boldsymbol{LC})^{-1}\boldsymbol{B} \tag{35}$$

$$\tilde{\boldsymbol{D}}(s) = \boldsymbol{I} - \boldsymbol{C}(s\boldsymbol{I} - \boldsymbol{A} + \boldsymbol{LC})^{-1}\boldsymbol{L} \tag{36}$$

$$\boldsymbol{X}(s) = \boldsymbol{I} + \boldsymbol{C}(s\boldsymbol{I} - \boldsymbol{A} + \boldsymbol{BF})^{-1}\boldsymbol{L} \tag{37}$$

$$\tilde{\boldsymbol{X}}(s) = \boldsymbol{I} + \boldsymbol{F}(s\boldsymbol{I} - \boldsymbol{A} + \boldsymbol{LC})^{-1}\boldsymbol{B} \tag{38}$$

$$\boldsymbol{Y}(s) = -\boldsymbol{F}(s\boldsymbol{I} - \boldsymbol{A} + \boldsymbol{BF})^{-1}\boldsymbol{L} \tag{39}$$

$$\tilde{\boldsymbol{Y}}(s) = -\boldsymbol{F}(s\boldsymbol{I} - \boldsymbol{A} + \boldsymbol{LC})^{-1}\boldsymbol{L} \tag{40}$$

It can be seen that the DCF representation of the DSA model is expressed by explicit formulas in terms of its state-space realisation. Hence, it is numerically easy to use.

doi: 10.1049/iet-cta.2010.0117

Now, to obtain (33)–(40) is reduced to choosing two gains $\boldsymbol{F}$ and $\boldsymbol{L}$ which actually represent the state feedback gain matrix and state estimator gain matrix of the DSA model, respectively. Since the DSA model is decoupled, the gains $\boldsymbol{F}$ and $\boldsymbol{L}$ can be partitioned as

$$\boldsymbol{F} = \left[\begin{array}{c|c} \boldsymbol{F_1} & 0 \\ \hline 0 & \boldsymbol{F_2} \end{array}\right], \quad \boldsymbol{L} = \left[\begin{array}{c} \boldsymbol{L_1} \\ \hline \boldsymbol{L_2} \end{array}\right] \tag{41}$$

Hence, we can individually design the gains for the VCM and PZT loops by using the pole placement method [19]. Since the gains $\boldsymbol{F}$ and $\boldsymbol{L}$ govern the characteristics of the nominal feedback control loop, they should be selected appropriately such that the PZT loop has a faster dynamics than the VCM loop and the estimator faster than the state feedback loop, and meanwhile sufficient stability robustness is provided.